Cite as: Sirohi *et al*., *Science*
10.1126/science.aaf5316 (2016).

# The 3.8 Å resolution cryo-EM structure of Zika virus

**Devika Sirohi,[1]* Zhenguo Chen,[1]* Lei Sun,[1] Thomas Klose,[1] Theodore C. Pierson,[2] Michael G. Rossmann,[1]† Richard J. Kuhn[1]†**

[1]Markey Center for Structural Biology and Purdue Institute for Inflammation, Immunology and Infectious Disease, Purdue University, West Lafayette, IN 47907, USA. [2]Viral Pathogenesis Section, Laboratory of Viral Diseases, National Institute of Allergy and Infectious Diseases, National Institutes of Health, Bethesda, MD 20892, USA.

*These authors contributed equally to this work.

†Corresponding authors. E-mail: mr@purdue.edu (M.G.R); kuhnr@purdue (R.J.K)

**The recent rapid spread of Zika virus and its unexpected linkage to birth defects and an autoimmune-neurological syndrome has generated worldwide concern. Zika virus is a flavivirus like dengue, yellow fever and West Nile viruses. We present the 3.8Å resolution structure of mature Zika virus determined by cryo-electron microscopy. The structure of Zika virus is similar to other known flavivirus structures except for the ~10 amino acids that surround the Asn154 glycosylation site found in each of the 180 envelope glycoproteins that make up the icosahedral shell. The carbohydrate moiety associated with this residue, recognizable in the cryo-EM electron density, may function as an attachment site of the virus to host cells. This region varies not only among Zika virus strains but also in other flaviviruses and suggests that changes in this region influence virus transmission and disease.**



The current Zika virus (ZIKV) epidemic in the Americas is linked to a sudden increase in the reported cases of congenital microcephaly and Guillain Barré syndrome. This has led the World Health Organization (WHO) in February 2016 to declare 'a public health emergency of international concern' (*1*). ZIKV was first discovered in a sentinel rhesus monkey in the Zika valley of Uganda in 1947 (*2*). It was subsequently isolated from mosquitos in 1948 (*2*) and from humans in 1952 (*3*). It is a re-emerging mosquito-transmitted virus that was relatively unknown until 2007 when it caused a major epidemic on Yap Island in Micronesia (*4*) followed by outbreaks in Oceania in 2013-14 (*5*). Following its introduction into Brazil in 2015 (*6*), the virus has spread rapidly across the Americas (*7*).

ZIKV belongs to the *Flaviviridae* family of positive strand RNA viruses that include human pathogens such as the mosquito transmitted dengue virus (DENV), West Nile virus (WNV), Japanese encephalitis virus (JEV), yellow fever virus (YFV) and tick-borne encephalitic virus (TBEV) (*8*). ZIKV causes a rash and a febrile flu-like illness in the majority of symptomatic individuals, but increasing evidence suggests a possibility of neurological abnormalities in the developing fetus (*9*, *10*) and paralysis in infected adults (*11*). In addition to transmission by mosquitoes, ZIKV may be sexually (*12*, *13*) and vertically transmitted (*9*, *10*). The structure, tropism and pathogenesis are largely unknown and are the focus of current investigations in an effort to address the need for rapid development of vaccines and therapeutics.

Flaviviruses are enveloped viruses containing an RNA genome of about 11,000 bases complexed with multiple copies of the capsid protein, surrounded by an icosahedral shell consisting of 180 copies of both the envelope (E) glycoprotein (~500 amino acids) and the membrane (M) protein (~75 amino acids) or the precursor membrane (prM) protein (~165 amino acids) anchored in a lipid membrane. The genome also codes for seven nonstructural proteins that are involved in replication, assembly, and antagonizing the host innate response to infection. In their life cycle, flavivirus virions exist in three major states, namely immature, mature and fusogenic, which are noninfectious, infectious and host membrane binding states, respectively (*8*). The virus is initially assembled in the endoplasmic reticulum as a noninfectious "spiky" immature particle consisting of 60 trimeric E:prM heterodimer spikes (*14*). Maturation into a mature, "smooth" virus consisting of 90 dimeric E:M heterodimers (*15*, *16*) occurs in the low pH environment of the trans-Golgi network through conformational changes of the surface glycoproteins and cleavage of prM into the pr peptide and M protein by the host protease furin. In the immature virus, the pr peptide protects the ~12 amino acid fusion loop on the E protein. Removal of the pr peptide in the maturation process exposes the fusion loop, priming the virus for low pH-mediated endosomal fusion (*17*). In addition to the aforementioned states, the structure of flavivirus virions can be influenced by temperature (*18*) and efficiency of prM cleavage resulting in a heterogeneous population of particles (*19*).

We report here the cryo-EM structure of the mature ZIKV at near atomic resolution (3.8Å) and compare it with the structure of other flaviviruses to provide a foundation for detailed analyses of the virology, antigenicity, and path-

ogenesis of this emerging threat to public health. ZIKV Strain H/PF/2013, isolated from an infected patient during the French Polynesia epidemic in 2013-14 (*20*), was grown and purified from mammalian cells at 37°C. It was shown recently that the coding region of this strain has >99.9% amino acid identity to the strain currently circulating in Latin America (*21*). Low passage Vero cells, derived from African green monkey kidney cells, were chosen for propagating the virus. To ensure a homogenous population of virions suitable for single particle reconstruction, virus was purified from Vero cells that overexpressed host protease furin (Vero-Furin). Vero-Furin ($10^9$) cells were infected with ZIKV at a multiplicity of infection (MOI) of 0.1. The virus was harvested under conditions of low cytopathic effect (CPE) and purified using polyethylene glycol-8000, 24% sucrose cushion ultracentrifugation, and a potassium tartrate (10-35%) / glycerol (7.5-26%) gradient as previously published (*17*). The identity of the virus was verified by RT-PCR and qRT-PCR (*22*); the primer sequences are shown in table S1.

The ZIKV preparation was frozen onto Lacey carbon EM grids and examined with an FEI Titan Krios EM equipped with a Gatan K2 Summit detector using a magnification of 14,000 in the "super-resolution" mode resulting in a pixel size of 1.04Å (Fig. 1A). The total exposure time for producing one image composed of 70 frames was 14 s and required a dose rate of 2 $e^-/Å^2$/sec. A total of 2,974 images were collected, and 64,518 particles were boxed using the automated Appion method (*23*). Non-reference 2D classification was performed with the Relion program (*24*) to select 20,151 particles. The data set was split into two subsets according to the Gold Standard convention (*25*). The jspr program (*26*) was used for initial model generation, refinement of the orientation and centering of the selected particles. After two rounds of 3D classification, 11,842 particles were used to generate a cryo-EM map at an average resolution of 4.2Å. Application of soft masks improved the overall resolution to 3.8Å, calculated using the 0.143 Fourier shell correlation (FSC) criterion (*25*) (Fig. 1D). The DENV2 structure (*16*) was used as a starting point for model building. The atomic model was built manually using the program Coot (*27*) and refined with Phenix (*28*) and CNS (*29*). The final cryo-EM density was Fourier analyzed. The resultant Fourier coefficients were used as targets for a "crystallographic" refinement. The final $R_{work}$ and $R_{free}$ were 38% and 39%, respectively (table S2). The map showed continuous density for the E and M polypeptide chains and large side chain densities were also visible in many cases, which was useful for sequence assignment. Except for the last three residues of E at its C terminus, all residues in both the E (1-501 residues) and M (1-75 residues) proteins were fitted into the density (Fig. 1E). A representative volume of density is shown in Fig. 1F. Similar to other flaviviruses, the E protein of ZIKV consists of four domains: the stem/transmembrane domain (E-S/ E-TM) that anchors the protein into the membrane and domains I, II and III that constitute the predominantly β-strand surface portion of the protein (Fig. 2). The M protein consists of a loop at the N terminus (M-Loop or soluble M), stem (M-S) and transmembrane (M-TM) regions consisting of 1 and 2 helices, respectively, which anchor the M protein to the lipid bilayer (see also figs. S1 and S2).

The cryo-EM map showed that the mature ZIKV structure was similar to mature DENV (*15*, *16*) and WNV structures (*30*) (Fig. 1). The radial distance of the core lipid bilayer and envelope ectodomains was similar to those of DENV2 (*16*) (Fig. 1C). A noticeable feature is the protruding density on the surface of the virus (red in Fig. 1, B and C), shown below to be the glycan on the E protein. The E proteins exhibited the characteristic "herringbone" structure in the virion, where there is one dimeric heterodimer $(E\text{-}M)_2$ located on each of thirty two-fold vertices and sixty dimeric heterodimers $(E\text{-}M)_2$ in general positions within the icosahedral protein shell (Fig. 1E). The root mean square deviation (r.m.s.d) between the equivalent Cα atoms of mature ZIKV and DENV E and M proteins was 1.8Å. However, by far the biggest difference (up to 6Å) between equivalent Cα atoms of these viruses is the region around the glycosylation site (Asn154 in ZIKV and Asn153 in DENV) (Fig. 3). ZIKV has a single glycosylation site in E protein (Asn154) whereas DENV is glycosylated at two sites within the E protein (Asn67 and Asn153) (fig. S2). Dendritic cell-specific intercellular adhesion molecule 3-grabbing non-integrin (DC-SIGN) and mannose receptor (MR) are putative DENV receptors binding to the glycan(s) (*31*, *32*). DC-SIGN was shown by cryo-EM to bind to the glycans at Asn67 on two neighboring E proteins of the mature virion (*31*).

The structures of various flaviviruses alone and their complexes with neutralizing antibodies (*33*) or cellular receptor (*31*) have been reported previously. These structures have demonstrated various mechanisms of antibody neutralization and receptor interactions. Carbohydrate moieties on the virus may be used for cell attachment and likely play a role in disease severity. For DENV, glycosylation at Asn67 on the E protein is an attachment site for several cell types shown to be relevant targets of infection in vivo (*31*, *32*). Similarly, glycosylation at Asn154 in WNV has been linked to neurotropism (*34*). These observations demonstrate the significance of glycosylation for attachment to cells in flaviviruses. The carbohydrate densities for ZIKV and DENV2 are not coincident and the conformation of their surrounding residues is different (Fig. 3). This region varies not only among ZIKV strains (*35*) but also in other flaviviruses and suggests that changes in this region influence local virus structure and possibly dynamics (Fig. 3D). In part, this is

because of an insertion of 5 residues in ZIKV relative to DENV (Fig. 3A) reflecting a highly variable region of the E protein. The glycan at E residue 154 is located on a loop that is adjacent to the fusion peptide in the neighboring E protein and may control solvent access to the fusion loop. The conserved fusion loop and the neighboring region is an epitope for numerous, cross-reactive antibodies that vary considerably in potency and sensitivity to the presence of uncleaved prM on the virion (*36*). The differences shown here may modulate the sensitivity of ZIKV to antibodies that bind the fusion loop epitopes. Furthermore, this region is perhaps also important for attachment to cellular lectin receptors. The differences in E protein structure shown here between ZIKV and other flaviviruses may govern cellular tropism and contribute to disease outcome.

## REFERENCES AND NOTES


1. World Health Organization (WHO), *Zika Strategic Response Framework & Joint Operations Plan (January-June 2016)* (WHO, 2016).
2. G. W. Dick, S. F. Kitchen, A. J. Haddow, Zika virus. I. Isolations and serological specificity. *Trans. R. Soc. Trop. Med. Hyg.* **46**, 509–520 (1952). Medline doi:10.1016/0035-9203(52)90042-4
3. F. N. MacNamara, Zika virus: A report on three cases of human infection during an epidemic of jaundice in Nigeria. *Trans. R. Soc. Trop. Med. Hyg.* **48**, 139–145 (1954). Medline doi:10.1016/0035-9203(54)90006-1
4. M. R. Duffy, T. H. Chen, W. T. Hancock, A. M. Powers, J. L. Kool, R. S. Lanciotti, M. Pretrick, M. Marfel, S. Holzbauer, C. Dubray, L. Guillaumot, A. Griggs, M. Bel, A. J. Lambert, J. Laven, O. Kosoy, A. Panella, B. J. Biggerstaff, M. Fischer, E. B. Hayes, Zika virus outbreak on Yap Island, Federated States of Micronesia. *N. Engl. J. Med.* **360**, 2536–2543 (2009). Medline doi:10.1056/NEJMoa0805715
5. V. M. Cao-Lormeau, C. Roche, A. Teissier, E. Robin, A. L. Berry, H. P. Mallet, A. A. Sall, D. Musso, Zika virus, French Polynesia, South Pacific, 2013. *Emerg. Infect. Dis.* **20**, 1085–1086 (2014). Medline doi:10.3201/eid2011.141380
6. C. Zanluca, V. C. Melo, A. L. Mosimann, G. I. Santos, C. N. Santos, K. Luz, First report of autochthonous transmission of Zika virus in Brazil. *Mem. Inst. Oswaldo Cruz* **110**, 569–572 (2015). Medline doi:10.1590/0074-02760150192
7. European Center for Disease Prevention and Control (ECDC), *Rapid Risk Assessment. Zika Virus Disease Epidemic: Potential Association with Microcephaly and Guillain–Barré Syndrome. Third Update, 23 February 2016* (ECDC, 2016).
8. B. D. Lindenbach, C. L. Murray, H.-J. Thile, C. M. Rice, "Flaviviridae: The Viruses and Their Replication," in *Fields Virology,* D. M. Knipe, P. M. Howley, Eds. (vol. 1, Lippincott Williams & Wilkins, 2013), pp. 1101–1152.
9. J. Mlakar, M. Korva, N. Tul, M. Popović, M. Poljšak-Prijatelj, J. Mraz, M. Kolenc, K. Resman Rus, T. Vesnaver Vipotnik, V. Fabjan Vodušek, A. Vizjak, J. Pižem, M. Petrovec, T. Avšič Županc, Zika virus associated with microcephaly. *N. Engl. J. Med.* **374**, 951–958 (2016). Medline doi:10.1056/NEJMoa1600651
10. R. B. Martines, J. Bhatnagar, M. K. Keating, L. Silva-Flannery, A. Muehlenbachs, J. Gary, C. Goldsmith, G. Hale, J. Ritter, D. Rollin, W. J. Shieh, K. G. Luz, A. M. Ramos, H. P. Davi, W. Kleber de Oliveria, R. Lanciotti, A. Lambert, S. Zaki, Notes from the field: Evidence of Zika virus infection in brain and placental tissues from two congenitally infected newborns and two fetal losses - Brazil, 2015. *MMWR Morb. Mortal. Wkly. Rep.* **65**, 159–160 (2016). Medline doi:10.15585/mmwr.mm6506e1
11. V.-M. Cao-Lormeau, A. Blake, S. Mons, S. Lastère, C. Roche, J. Vanhomwegen, T. Dub, L. Baudouin, A. Teissier, P. Larre, A. L. Vial, C. Decam, V. Choumet, S. K. Halstead, H. J. Willison, L. Musset, J. C. Manuguerra, P. Despres, E. Fournier, H. P. Mallet, D. Musso, A. Fontanet, J. Neil, F. Ghawché, Guillain-Barré Syndrome outbreak associated with Zika virus infection in French Polynesia: A case-control study. *Lancet* (2016). Medline doi:10.1016/S0140-6736(16)00562-6
12. B. D. Foy, K. C. Kobylinski, J. L. Chilson Foy, B. J. Blitvich, A. Travassos da Rosa, A. D. Haddow, R. S. Lanciotti, R. B. Tesh, Probable non-vector-borne transmission of Zika virus, Colorado, USA. *Emerg. Infect. Dis.* **17**, 880–882 (2011). Medline doi:10.3201/eid1705.101939
13. D. Musso, C. Roche, E. Robin, T. Nhan, A. Teissier, V. M. Cao-Lormeau, Potential sexual transmission of Zika virus. *Emerg. Infect. Dis.* **21**, 359–361 (2015). Medline doi:10.3201/eid2102.141363
14. Y. Zhang, J. Corver, P. R. Chipman, W. Zhang, S. V. Pletnev, D. Sedlak, T. S. Baker, J. H. Strauss, R. J. Kuhn, M. G. Rossmann, Structures of immature flavivirus particles. *EMBO J.* **22**, 2604–2613 (2003). Medline doi:10.1093/emboj/cdg270
15. R. J. Kuhn, W. Zhang, M. G. Rossmann, S. V. Pletnev, J. Corver, E. Lenches, C. T. Jones, S. Mukhopadhyay, P. R. Chipman, E. G. Strauss, T. S. Baker, J. H. Strauss, Structure of dengue virus: Implications for flavivirus organization, maturation, and fusion. *Cell* **108**, 717–725 (2002). Medline doi:10.1016/S0092-8674(02)00660-8
16. X. Zhang, P. Ge, X. Yu, J. M. Brannan, G. Bi, Q. Zhang, S. Schein, Z. H. Zhou, Cryo-EM structure of the mature dengue virus at 3.5-Å resolution. *Nat. Struct. Mol. Biol.* **20**, 105–110 (2013). Medline doi:10.1038/nsmb.2463
17. I. M. Yu, W. Zhang, H. A. Holdaway, L. Li, V. A. Kostyuchenko, P. R. Chipman, R. J. Kuhn, M. G. Rossmann, J. Chen, Structure of the immature dengue virus at low pH primes proteolytic maturation. *Science* **319**, 1834–1837 (2008). Medline doi:10.1126/science.1153264
18. X. Zhang, J. Sheng, P. Plevka, R. J. Kuhn, M. S. Diamond, M. G. Rossmann, Dengue structure differs at the temperatures of its human and mosquito hosts. *Proc. Natl. Acad. Sci. U.S.A.* **110**, 6795–6799 (2013). Medline doi:10.1073/pnas.1304300110
19. T. C. Pierson, M. S. Diamond, Degrees of maturity: The complex structure and biology of flaviviruses. *Curr. Opin. Virol.* **2**, 168–175 (2012). Medline doi:10.1016/j.coviro.2012.02.011
20. C. Baronti, G. Piorkowski, R. N. Charrel, L. Boubis, I. Leparc-Goffart, X. de Lamballerie, Complete coding sequence of Zika virus from a French Polynesia outbreak in 2013. *Genome Announc.* **2**, e00500-14 (2014). Medline doi:10.1128/genomeA.00500-14
21. A. Enfissi, J. Codrington, J. Roosblad, M. Kazanji, D. Rousset, Zika virus genome from the Americas. *Lancet* **387**, 227–228 (2016). Medline doi:10.1016/S0140-6736(16)00003-9
22. R. S. Lanciotti, O. L. Kosoy, J. J. Laven, J. O. Velez, A. J. Lambert, A. J. Johnson, S. M. Stanfield, M. R. Duffy, Genetic and serologic properties of Zika virus associated with an epidemic, Yap State, Micronesia, 2007. *Emerg. Infect. Dis.* **14**, 1232–1239 (2008). Medline
23. G. C. Lander, S. M. Stagg, N. R. Voss, A. Cheng, D. Fellmann, J. Pulokas, C. Yoshioka, C. Irving, A. Mulder, P. W. Lau, D. Lyumkis, C. S. Potter, B. Carragher, Appion: An integrated, database-driven pipeline to facilitate EM image processing. *J. Struct. Biol.* **166**, 95–102 (2009). Medline doi:10.1016/j.jsb.2009.01.002
24. S. H. Scheres, RELION: Implementation of a Bayesian approach to cryo-EM structure determination. *J. Struct. Biol.* **180**, 519–530 (2012). Medline
25. P. B. Rosenthal, R. Henderson, Optimal determination of particle orientation, absolute hand, and contrast loss in single-particle electron cryomicroscopy. *J. Mol. Biol.* **333**, 721–745 (2003). Medline doi:10.1016/j.jmb.2003.07.013
26. F. Guo, W. Jiang, Single particle cryo-electron microscopy and 3-D reconstruction of viruses. *Methods Mol. Biol.* **1117**, 401–443 (2013). Medline doi:10.1007/978-1-62703-776-1_19
27. P. Emsley, B. Lohkamp, W. G. Scott, K. Cowtan, Features and development of Coot. *Acta Crystallogr. D Biol. Crystallogr.* **66**, 486–501 (2010). Medline doi:10.1107/S0907444910007493
28. P. V. Afonine, R. W. Grosse-Kunstleve, N. Echols, J. J. Headd, N. W. Moriarty, M. Mustyakimov, T. C. Terwilliger, A. Urzhumtsev, P. H. Zwart, P. D. Adams, Towards automated crystallographic structure refinement with *phenix.refine*. *Acta Crystallogr. D Biol. Crystallogr.* **68**, 352–367 (2012). Medline doi:10.1107/S0907444912001308
29. A. T. Brünger, P. D. Adams, G. M. Clore, W. L. DeLano, P. Gros, R. W. Grosse-Kunstleve, J. S. Jiang, J. Kuszewski, M. Nilges, N. S. Pannu, R. J. Read, L. M. Rice, T. Simonson, G. L. Warren, Crystallography & NMR system: A new software suite for macromolecular structure determination. *Acta Crystallogr. D Biol. Crystallogr.* **54**, 905–921 (1998). Medline doi:10.1107/S0907444998003254
30. S. Mukhopadhyay, B. S. Kim, P. R. Chipman, M. G. Rossmann, R. J. Kuhn,

Structure of West Nile virus. *Science* **302**, 248 (2003). Medline doi:10.1126/science.1089316
31. E. Pokidysheva, Y. Zhang, A. J. Battisti, C. M. Bator-Kelly, P. R. Chipman, C. Xiao, G. G. Gregorio, W. A. Hendrickson, R. J. Kuhn, M. G. Rossmann, Cryo-EM reconstruction of dengue virus in complex with the carbohydrate recognition domain of DC-SIGN. *Cell* **124**, 485–493 (2006). Medline doi:10.1016/j.cell.2005.11.042
32. J. L. Miller, B. J. de Wet, L. Martinez-Pomares, C. M. Radcliffe, R. A. Dwek, P. M. Rudd, S. Gordon, The mannose receptor mediates dengue virus infection of macrophages. *PLOS Pathog.* **4**, e17 (2008). Medline doi:10.1371/journal.ppat.0040017
33. S. M. Lok, The interplay of dengue virus morphological diversity and human antibodies. *Trends Microbiol.* 10.1016/j.tim.2015.12.004 (2015). Medline
34. D. W. Beasley, M. C. Whiteman, S. Zhang, C. Y. Huang, B. S. Schneider, D. R. Smith, G. D. Gromowski, S. Higgs, R. M. Kinney, A. D. Barrett, Envelope protein glycosylation status influences mouse neuroinvasion phenotype of genetic lineage 1 West Nile virus strains. *J. Virol.* **79**, 8339–8347 (2005). Medline doi:10.1128/JVI.79.13.8339-8347.2005
35. O. Faye, C. C. Freire, A. Iamarino, O. Faye, J. V. de Oliveira, M. Diallo, P. M. Zanotto, A. A. Sall, Molecular evolution of Zika virus during its emergence in the 20th century. *PLOS Negl. Trop. Dis.* **8**, e2636 (2014). Medline doi:10.1371/journal.pntd.0002636
36. S. Nelson, C. A. Jost, Q. Xu, J. Ess, J. E. Martin, T. Oliphant, S. S. Whitehead, A. P. Durbin, B. S. Graham, M. S. Diamond, T. C. Pierson, Maturation of West Nile virus modulates sensitivity to antibody-mediated neutralization. *PLOS Pathog.* **4**, e1000060 (2008). Medline doi:10.1371/journal.ppat.1000060
37. W. Liu, Y. Xie, J. Ma, X. Luo, P. Nie, Z. Zuo, U. Lahrmann, Q. Zhao, Y. Zheng, Y. Zhao, Y. Xue, J. Ren, IBS: An illustrator for the presentation and visualization of biological sequences. *Bioinformatics* **31**, 3359–3361 (2015). Medline doi:10.1093/bioinformatics/btv362
38. F. Sievers, A. Wilm, D. Dineen, T. J. Gibson, K. Karplus, W. Li, R. Lopez, H. McWilliam, M. Remmert, J. Söding, J. D. Thompson, D. G. Higgins, Fast, scalable generation of high-quality protein multiple sequence alignments using Clustal Omega. *Mol. Syst. Biol.* **7**, 539 (2011). Medline doi:10.1038/msb.2011.75

## ACKNOWLEDGMENTS

We thank Pr. Xavier de Lamballerie (Emergence des Pathologies Virales, Aix-Marseille Université, Marseille, France) and the European Virus Archive goes Global (EVAg) for consenting to the use of H/PF/2013 ZIKV strain for this study under a material transfer agreement with the EVAg parter, Aix-Marseille Université, and Michael S. Diamond (Washington University, St. Louis, USA) for sending the virus. We acknowledge Elizabeth Frye for help with sequence alignments. We are grateful to Wen Jiang for his jspr program to perform the anisotropic magnification corrections and Yue Liu for providing help in submitting the PDB coordinates. The work presented in this report was funded by the National Institute of Allergy and Infectious Diseases of the National Institutes of Health through grants R01AI073755 and R01AI076331 awarded to M.G.R. and R.J.K. T.C.P was supported by the intramural program of the National Institute of Allergy and Infectious Diseases. Supporting information for this research is provided in the supplementary materials. The atomic coordinates and cryo-EM density maps for the mature ZIKV are available at the Protein Data Bank and Electron Microscopy Data Bank via accession codes (5IRE) and (EMD-8116), respectively.

## SUPPLEMENTARY MATERIALS

www.sciencemag.org/cgi/content/full/science.aaf5316/DC1
Figs. S1 and S2
Tables S1 and S2
References (*37*, *38*)

4 March 2016; accepted 21 March 2016
Published online 31 March 2016
10.1126/science.aaf5316

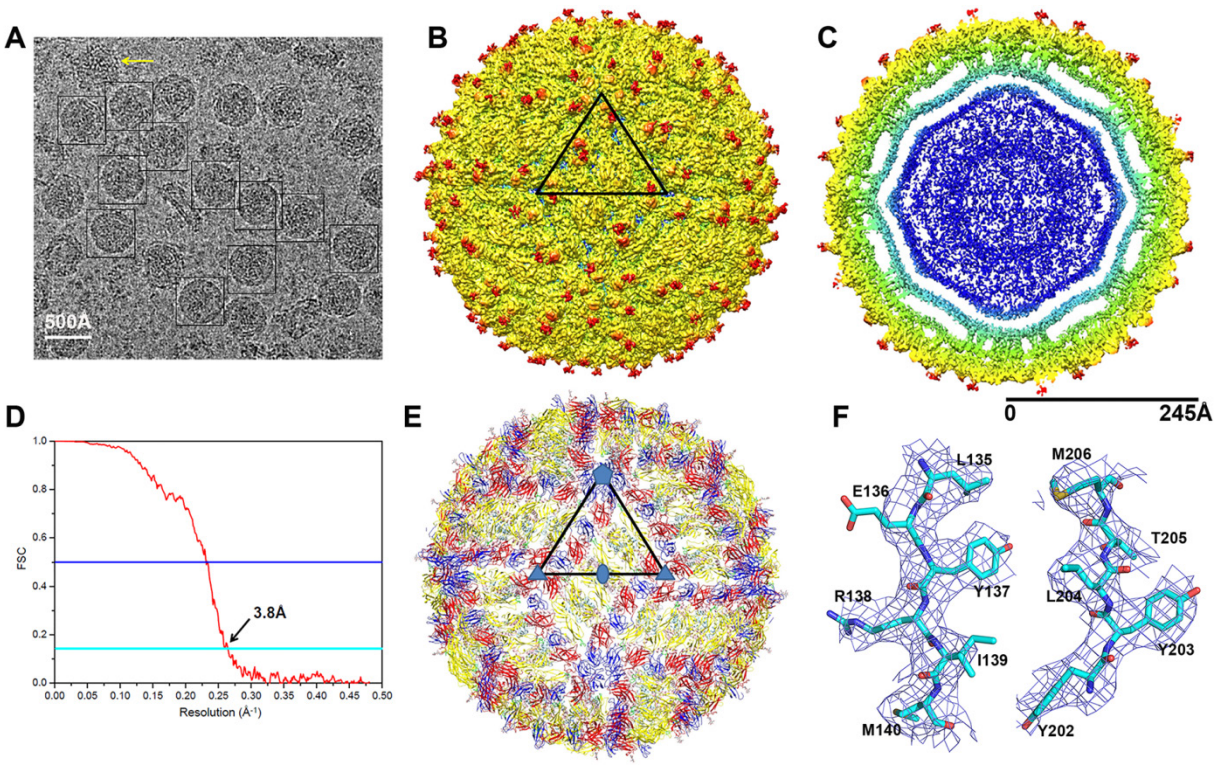


**Fig. 1. The cryo-EM structure of Zika virus at 3.8Å.** (**A**) A representative cryo-EM image of frozen, hydrated ZIKV showing the distribution of virion phenotypes. Smooth, mature virus particles are identified by a surrounding black box. A partially mature virus particle is identified by the yellow arrow. (**B**) A surface-shaded depth cued representation of ZIKV viewed down the icosahedral two-fold axis. The asymmetric unit is identified by the black triangle. (**C**) A cross-section of ZIKV showing the radial density distribution. Panels B and C are color-coded based on the following radii: up to 130Å, blue; 131Å to 150Å, cyan; 151Å to 190Å, green; 191Å to 230Å, yellow, from 231Å, red. The region shown in blue fails to follow icosahedral symmetry and therefore its density is uninterruptable as is the case with other flaviviruses. (**D**) A plot of the Fourier shell coefficient (FSC). Based on the 0.143 criterion for the gold standard comparison of two independent data sets, the resolution of the reconstruction is 3.8Å. The *x* axis shows 1/resolution in $Å^{-1}$; the *y* axis shows the FSC value. (**E**) The Cα backbone of the E and M proteins in the icosahedral ZIKV particle (same orientation as in Panel B above) showing the herringbone organization. The color code fits the standard designation of E protein domains I (red), domain II (yellow) and domain III (blue). (**F**) Representative cryo-EM electron densities of several amino acids of the E protein.

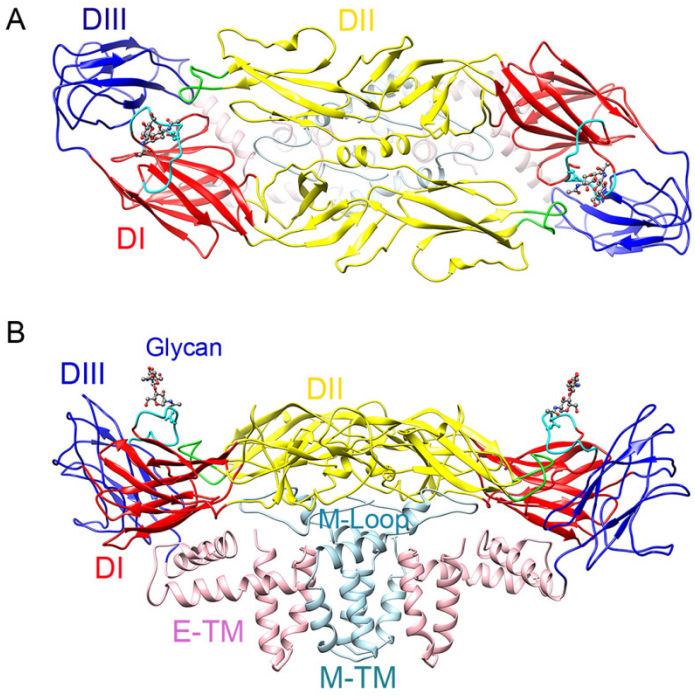


**Fig. 2. The structures of Zika virus E and M proteins.** (**A**) The E protein dimer is shown in ribbon form viewed down the two-fold axis. The color code fits the standard designation of E protein domains I (red), domain II (yellow) and domain III (blue). The underlying stem and transmembrane residues are shown (pink). The fusion loop (green; fig. S1), Asn154 glycan, and the variable loop surrounding the Asn154 glycan (residues 145-160, cyan) are highlighted. (**B**) Side view of the E-M dimer showing the three E ectodomains as well as the E stem/transmembrane domains (pink) and the M loop and stem/transmembrane domains (light blue). The E and M transmembrane domains are found within the lipid bilayer (Fig. 1C). All residues of M (1-75) and all but three residues of E (1-501) were identified in the density. The Asn154 glycan from one monomer is labeled and can be seen projecting from the surface.

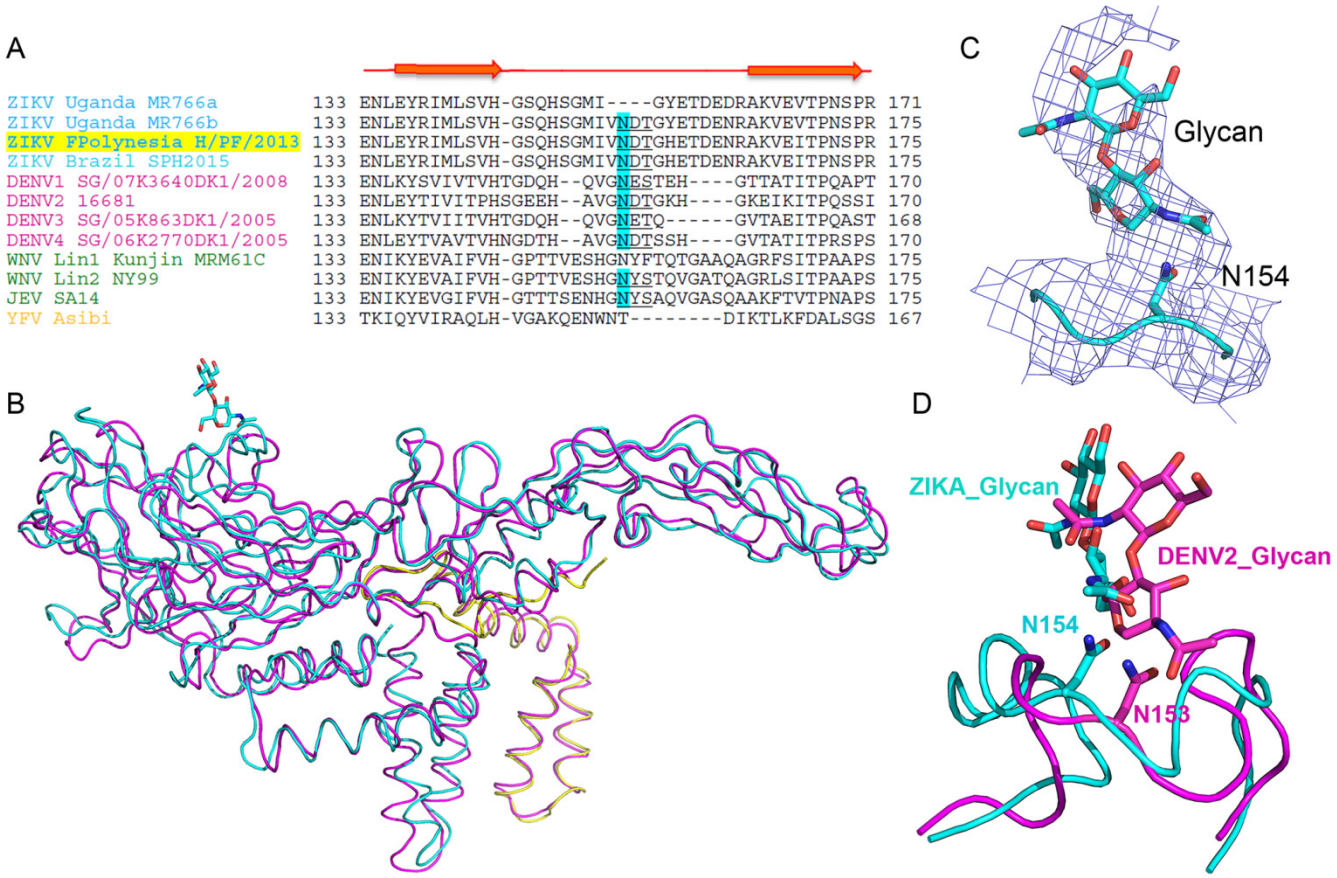


**Fig. 3. Comparison of E protein of Zika virus and other flaviviruses.** (**A**) The region of the E protein of ZIKV (H/PF/2013) along with other ZIKV strains is aligned to representative mosquito-transmitted flaviviruses. Approximately 40 residues of Domain 1 centered on the Asn154 glycosylation site are compared. The conserved glycosylation site at Asn153/154 is highlighted in blue. Red arrows represent secondary structures of ZIKV (sheets). The glycosylation motif N-X-S/T is underlined. The sequences for various flaviviruses were obtained from the Virus Pathogen Database and Analysis Resource (ViPR). Virus strains for which structural information was available were chosen where possible. GenBank Genome Accession codes for these viruses are as follows- ZIKV_Uganda_MR766(a): AY632535, ZIKV_Uganda_MR766(b): KU720415; ZIKV_FPolynesia_H/PF/2013: KJ776791; ZIKV_ Brazil_SPH2015: KU321639; DENV 1_SG/07K3640DK1/2008: GQ398255; DENV 2_16681: NC_001474; DENV 3_SG/05K863DK1/2005: EU081190; DENV4_SG/06K2270DK1/2005: GQ398256; WNV_Lineage1_Kunjin_MRM61C: D00246; WNV_Lineage2_NY99: DQ211652; JEV_SA14: D90194 and YFV_Asibi: AY640589. Sequence of the original isolate (ZIKV_MR766) varies based on the information source; it remains unclear whether this strain was glycosylated at N154 at the time of isolation or whether the glycosylation was acquired during passage through mouse brain. The sequences were manually aligned based on the structures of ZIKV and DENV2. (**B**) Superposition of the Cα backbone of the ZIKV and DENV 2 E and M proteins. The DENV 2 proteins are shown in magenta while the ZIKV E protein is shown in cyan and the M protein in yellow. (**C**) Electron density representing the glycan at Asn154. (**D**) Superposition of the loop region surrounding the glycosylation site (ZIKV: 144 -166; DENV2: 144 -161) flanking the Asn154 glycan for ZIKV (cyan) and DENV2 (magenta).